STREAM

IST-1999-10341

STREAM Consortium:
CNR-LAMEL/ST-MICROELECTRONICS/ /ISEN/SOFT IMAGING SYSTEM/ UNIVERSITY OF SHEFFIELD /IMEC/CNR-IESS/ UNIVERSITY OF PERUGIA

DELIVERABLE D4
Work packages nr. 2, Task 2.2 and 2.3
Partners UniPg, ISEN
Coordinator ST-Microelectronics

1ST report on physical characterisation of samples for stress measurements

Main authors:	Paolo Colpani, Giovanni Carlotti		
Contributing Author(s):	V.Senez		
Date:	17 – 07 – 2000	***Doc.No:***	IST10341-ST-RP002
Keywords:	STI, OXIDE, NITRIDE, FILLING, STRESS, BRILLOUIN		
Distribution list:	Mr. B.Netange (EEC) Armigliato, G. Carnevale, V. Senez, T. Schilling, A.G. Cullis, I. de Wolf, S. Lagomarsino, G.Carlotti		

Table of contents

1. Introduction p3

2. Process flow and materials for STI p3

3. Film characterization at ST p4

3.1 Intrinsic stress p6

3.2 Stress vs. T p7

3.2.1 TEOS p7

3.2.2 HDP oxide p8

3.2.3 Silicon Nitride p9

3.3 Stress vs. Time p10

4. Elastic characterization of film at UniPg p10

4.1 Experimental apparatus: the tandem-multipass Fabry-Perot interferometer p11

4.2 Guided acoustic modes p13

4.3 Measured spectra p14

4.4 Evaluation of the film elastic constants p16

5. Conclusion p19

6. References p19

7. Acknowledgments p19

1. Introduction

Aim of this deliverable is to report the film characterization done on the materials used to Shallow Trench Isolation (STI) formation. In particular the films used during the first measurement campaign [1] have been investigated to extract the necessary parameters for simulation. In the following sections of this document it will be presented the different characterizations done. Unfortunately some problems on sample preparation (ST is changing its 6" wafer pilot line to 8") and characterization (Brillouin light scattering technique needs very thick samples) did not allow to extract a complete characterization for all the films.

2. Process flow and materials for STI

A general STI process flow has been described in the chapter 3 of IST10341-ST-PR001 document. The STI samples prepared during the first measurement campaign followed the process flow reported in the table 1.

	Process steps	**Description**	**Type of film**
OP. 1	Pad oxidation	130 Å	Thermal oxide
OP. 2	Nitride deposition	split 120nm vs 160nm	LPCVD[1] Nitride
OP. 3	Active area definition	Litho + Etch (Nitride patterning and Silicon digging)+ resist removal	Std dry etching
OP. 4	Sidewall oxidation	300 Å	Thermal oxide
OP. 5	1st Oxide deposition: gap fill	400 nm of High Density Plasma oxide	HDP[2] oxide high D/S[3]
OP. 6	2nd Oxide deposition	Split between TEOS and HDP	TEOS oxide by a LPCVD furnace, HDP oxide low D/S
OP. 7	Oxide densification	Thermal treatment in N2 ambient	High Temperature anneal

Tab.1

Samples for strain characterization have been sorted after Op.6 and after Op.7.

The picture 1 shows an example of the final kind of STI obtained with different STI filling: full HDP vs. HDP plus TEOS.

[1] LPCVD means Low Pressure Chemical Vapor Deposition
[2] HDP means High Density Plasma deposition technique
[3] D/S means Deposition Sputtering ratio

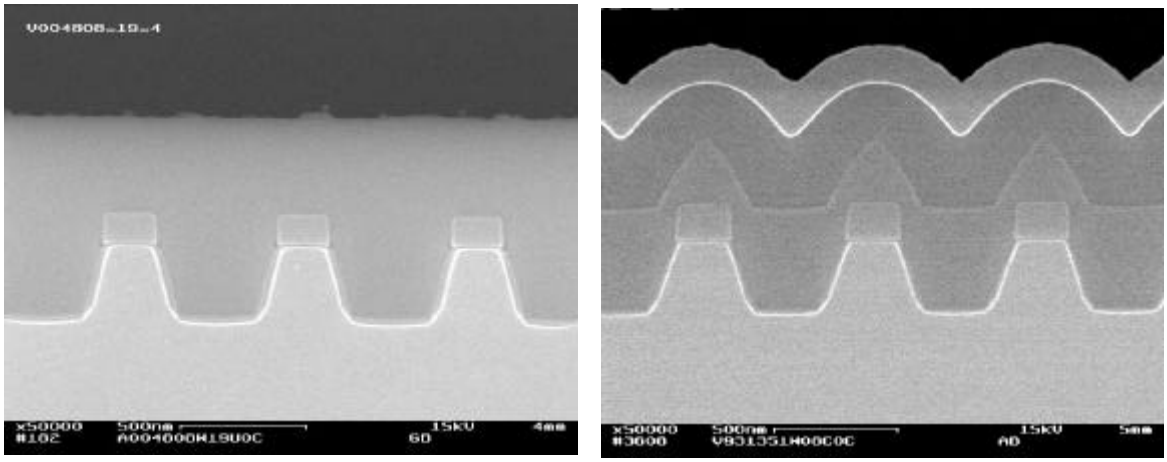

Picture 1. On the left, STI cross-section after full HDP oxide filling. On the right the same structure with HDP plus TEOS oxide filling. A poly cap layer has been deposited on the right sample.

In order to simulate the STI formation and the impact of the different process steps on silicon strain it has been necessary to characterize the following films:

- LPCVD Nitride
- HDP oxide with high D/S
- HDP oxide with low D/S
- LPCVD TEOS oxide

All the films have been studied before and after the oxide densification process step. It was established not useful to investigate in depth the characteristics of thermal oxide (Sidewall oxidation, pad oxidation) because the thermal oxide elastic film properties are well known.

3. Film characterization at ST

Six inches mono silicon wafers have been used like substrate for different film deposition. After deposition, the film thickness has been measured using a TENCOR UV 1250 equipped with a spectroscopic elipsometer and a reflectometer.

The silicon wafers were weighted before and after film deposition to determinate the film density. This density is obtained with the following equation,

$$D = (W_f - W_0)/(At) \qquad (1)$$

where:

D is the density, W_f is the wafer mass after film deposition, W_0 the wafer mass before film deposition, A is the wafer area and t is the film thickness

The wafer bow before and after film deposition was measured to calculate the intrinsic stress of the film by means of the FLX 2400 thin films stress measurement system by TENCOR. The FLX thin film stress measuring apparatus measures the changes in the radius of curvature of a substrate created by deposition of a stressed thin film on its surface. The stress in the thin film is calculated from the substrate radius of curvature using the following equation:

$$s = EH^2/[(1-c)6Rt] \quad (2)$$

where:

$E/(1-c)$ is the biaxial elastic modules of the substrate (1.8E11Pa for 100 silicon wafer); H is the substrate thickness; t is the film thickness; R is the substrate radius of curvature; s is the average film stress.

For LPCVD samples (Nitride and TEOS) it was necessary to remove the wafer backside deposition to obtain a reliable measure. The intrinsic stress measurement has been repeated after a convenient period of time (two months) to evaluate the stress modification due to water adsorption (extrinsic stress).

After the film deposition it was possible to measure the stress as a function of the temperature using the same stress measuring apparatus (FLX 2400). The variation of the radius of curvature of the wafer has been measured as a function of wafer temperature. It was possible to perform thermal cycles between room and 800°C temperature fixing the maximum temperature, the temperature ramp rate (up and down) and the number of observations. The temperature ramp rate is reported in the figure 1. The experimental ramp rate has been 3.5 °C/min during heating and 2.5°C/min during cooling.

Figure 1 Temperature profile during stress/temperature measurements on three different samples.

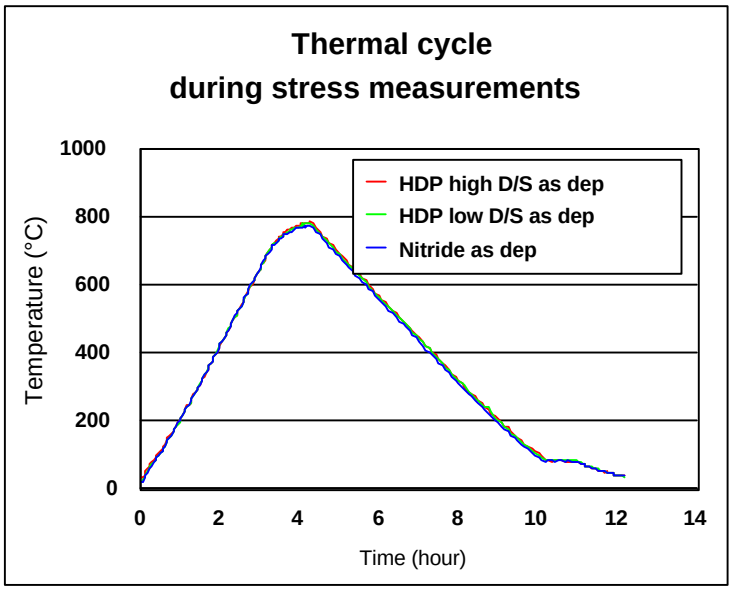

3.1 Intrinsic stress

In the table 2 the main parameters of the film characterized are reported.

Wafer code	FILM	Thickness (Å± 1s)	Density (g/cm3)	Intrinsic stress (dyne/cm2)
Perugia 2	SiO_2 by LPCVD TEOS	4830±84	2.37	-4.420E+08
Perugia 3	as previous plus High T anneal	4431±69	2.70	-2.880E+09
Perugia 5	SiO_2 from HDP (SiH_4,O_2,Ar) High D/S	4263±48	2.58	-1.390E+09
Perugia 6	as previous plus High T anneal	4264±44	2.55	-2.880E+09
Perugia 8	SiO_2 da HDP (SiH_4,O_2,Ar) Low D/S	4412±67	2.40	-1.380E+09
Perugia 9	as previous plus High T anneal	4319±59	2.49	-2.860E+09
Perugia 11	Si_3N_4 da LPCVD (NH_3/DCS)	2054±36	3.29	1.237E+10
Perugia 12	as previous plus High T anneal	2026±37	3.50	1.208E+10

Tab.2

It is possible to draw some comments on the basis of these data.

All the oxide films after high temperature annealing are very similar (same intrinsic compressive stress) and they look like a thermal oxide [Ref 1]. The TEOS oxide shows a considerable shrinkage during high temperature anneal. The different Deposition/Sputtering ratio does not influence the quality of HDP oxides. At the end

LPCVD nitride show a noticeable stability versus thermal treatment. The intrinsic stress of nitride is tensile.

3.2 Stress vs. temperature

This kind of measurement is useful to determinate the film thermal expansion coefficient in those regions where an elastic behavior is found. The stress change with temperature in the elastic range is governed by the following equation [2]:

$$d\sigma/dT = [E/(1-c)]_f*(\alpha_s-\alpha_f) \qquad (3)$$

where, $d\sigma/dT$ is the derivative of stress vs. temperature, $[E/(1-c)]_f$ is the biaxial module of the film, α_s and α_f are respectively the thermal expansion coefficients for the substrate and for the film. The equation above has two unknowns α_f and $[E/(1-c)]_f$. The biaxial module of the film was measured by the laboratories of Perugia University, while the derivative of stress vs. temperature has been measured with FLX 2400 equipment in ST 6" pilot line.

3.2.1 TEOS

The figure 2 shows TEOS stress versus temperature before and after high temperature anneal. It is possible to note that large isteresis is present for the film before high T anneal. After anneal the film seems to be in an elastic regime for the whole temperature range

Figure 2 Stress vs. Temperature for TEOS oxide before and after high temperature densification

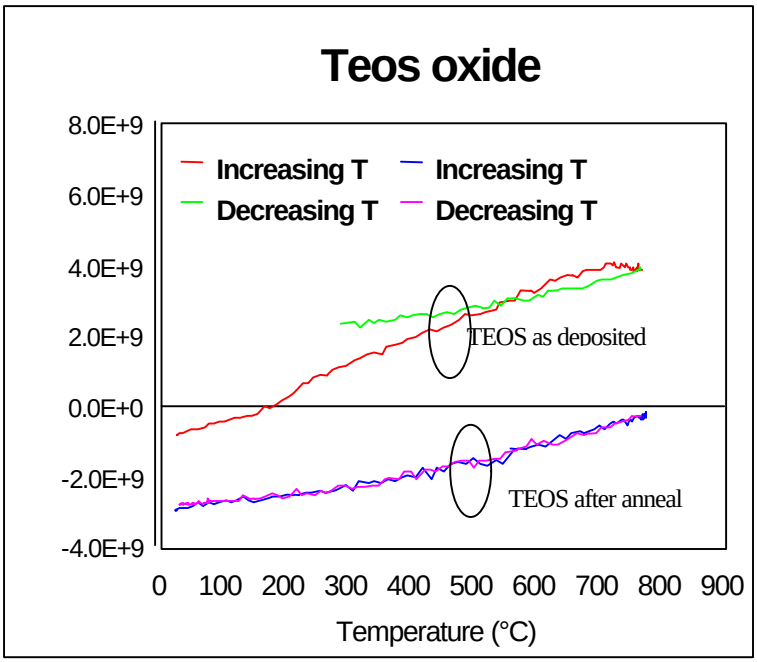

3.2.2 HDP oxide

The figure 3 shows HDP oxide stress (high D/S) versus temperature before and after oxide densification. The film, also after deposition, does not show the large isteresis just seen on TEOS oxide. Also the derivative of the stress it is not so different before and after high temperature anneal.

The figure 4 shows a comparison between TEOS and two type of HDP oxide (low and high D/S. Practically no difference behavior is present among HDP oxides with different D/S ratio. Moreover after anneal also the stress vs. temperature curves show no difference among TEOS and HDP oxide films.

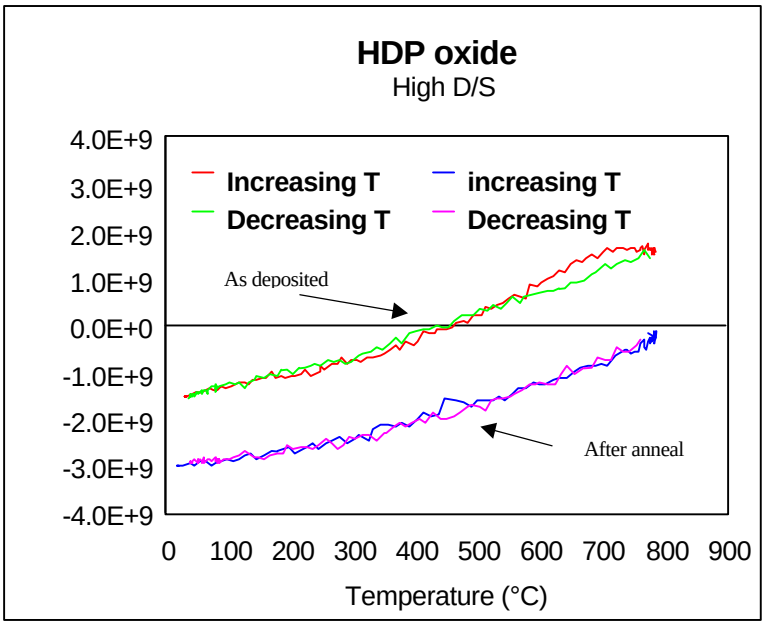

Figure 3 Stress versus temperature for HDP with high D/S oxide before and after anneal

Figure 4 Oxide films comparison. After deposition HDP oxides with different D/S show the same Stress vs. temperature curves. After anneal also TEOS oxide results very similar to HDP oxide

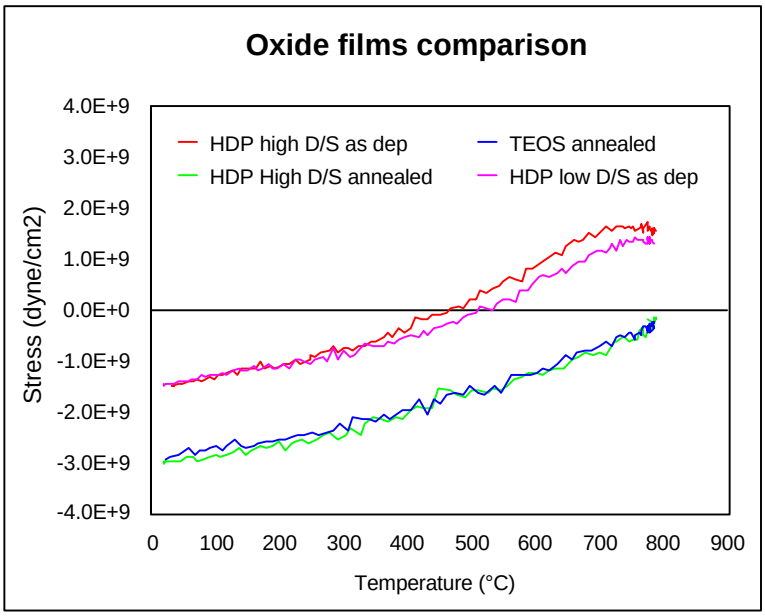

3.2.3 Silicon Nitride

The stress vs. temperature curves for silicon nitride are reported in the figure 5. In case of nitride, the stress variation with the temperature is negligible. These fact suggests that coefficients of linear thermal expansion of nitride and silicon are quite similar. These data are in good agreement with the data reported in the models of SSUPREM4 simulation program [3], where linear thermal expansion coefficients are $3.0*10^{-6}$ and $[3.052*10^{-6}+2*6.206*10^{-10}*(T-293)]$ respectively for nitride and silicon.

Figure 5 Stress vs. temperature curves for silicon nitride before and after high temperature anneal.

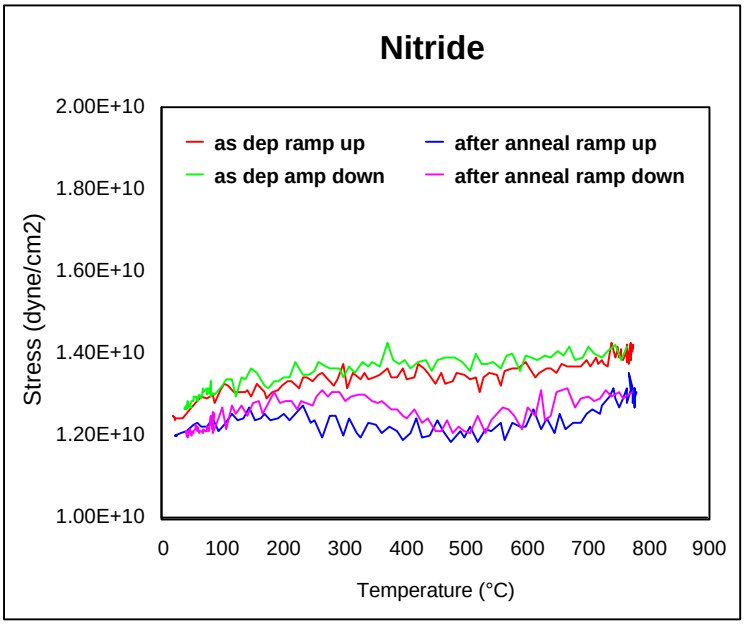

3.3 Stress vs. Time

The table 3 reports the room temperature film stresses measured after sample preparation and the same data obtained two months later.

Sample	**Stress (dyne/cm2)**	**Stress two month later (dyne/cm2)**
TEOS as dep.	-4.424E8	-8.067E8
TEOS annealed	-2.882E9	-2.992E9
HDP high D/S as dep.	-1.387E9	-1.443E9
HDP high D/S annealed	-2.88E9	-2.911E9
HDP low D/S as dep.	-1.278E9	-1.345E9
HDP low D/S annealed	-2.851E9	-2.829E9
Silicon nitride as dep.	1.237E10	1.227E10
Silicon nitride annealed	1.207E10	1.191E10

Tab.3

It has to be noted that only for TEOS not annealed a variation of the room temperature film stress is present. Therefore only for TEOS oxide after deposition the stress modification versus time has been studied. The figure 6 shows the stress variation versus time for a TEOS not annealed sample.

Figure 6 Stress versus time for a TEOS not annealed sample

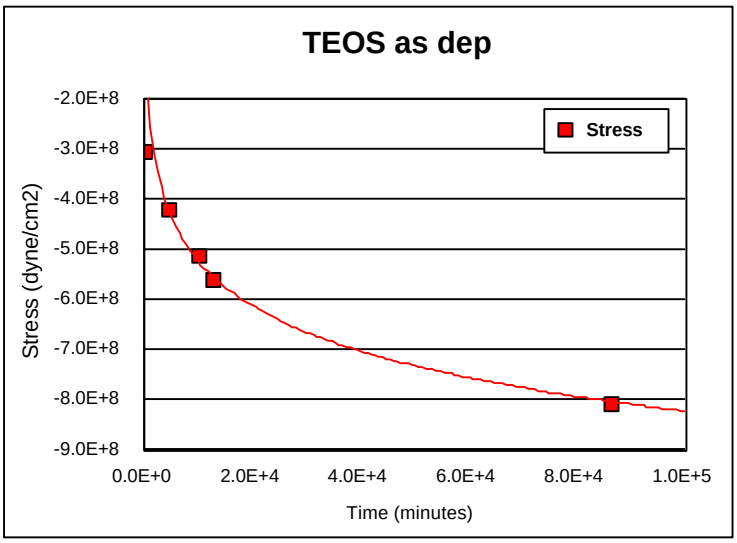

4. Elastic characterization of film at UniPg

During this first part of the project, the Brillouin light scattering (BLS) technique has been exploited in order to reveal the phase velocity of guided surface

acoustic modes in different silicate glass films deposited on Si substrates (first six specimens of Table 2). Before presenting the measured Brillouin spectra, let us recall the main features of the experimental apparatus and of the theory of light scattering from guided acoustic modes in thin films.

4.1 Experimental apparatus: the tandem-multipass Fabry-Perot interferometer

In a typical Brillouin scattering experiment one measures acoustic phonons with frequencies in the range between about 1 and 150 GHz. In order to extract the weak inelastic component of light from the elastically scattered contribution, a high-resolution spectrometer is required. To this aim, the best combination of high resolution and good throughput is achieved using a Fabry-Perot interferometer (FPI) as a scanning spectrometer. This system consists of two very flat mirrors mounted accurately parallel to each other with a variable spacing. For a fixed distance L_1 the interference condition is such that only light of wavelength L_1 will be transmitted, with $L_1=m\ L_1/2$ where m is an integer. Therefore, this instrument acts as a band-pass frequency filter whose peak transmission is close to unity over a narrow spectral interval, as shown in Fig.1. However, one has different interference orders which are separated in frequency by $c/2L_1$ Hz. This inter-order spacing is called the free spectral range (FSR). The width of the transmission peak determines the resolution of the instrument. The ratio of the FSR to the width is known as the finesse F, whose value depends on the mirror reflectivity R, although instrumental aperture and mirror flatness are also important parameters. In practice, the finesse is limited to values less than about 100 and this places an upper limit on the possible contrast, where the contrast C is the ratio of maximum to minimum transmission given by:

$$C = 1 + \frac{4F^2}{p^2} \leq 10^4 \qquad (4)$$

In thin films, it is usual that the elastically scattered light exceeds the intensity of the Brillouin component by more than a factor of 10^4-10^5, so that the above contrast is not sufficient for measuring in such a situation. A way for increasing the spectral contrast is the introduction of the multi-pass operation: by sending back a few times the light

through the same interferometer, the contrast can be increased up to values close to 10^{10} and this is sufficient for Brillouin scattering experiments in opaque materials.

In order to avoid the overlap of neighbouring interference order and extend the range of frequency investigated, it is possible to combine two interferometers of unequal mirror spacing (tandem operation), as shown in Fig. 7. The first interferometer of spacing L_1 transmits wavelengths

$$\Lambda_1 = 2L_1/m_1 \quad (5a)$$

for integral m_1, while the second interferometer of spacing L_2 transmits wavelengths

$$\Lambda_2 = 2L_2/m_2 \quad (5b)$$

for integral m_2.

Only if $L_1 = L_2$ light will be transmitted through the combination. It is important to notice, however, that to scan the transmitted wavelength, it is necessary to increment the mirror spacings L_1 and L_2 by DL_1, and DL_2 such that:

$$DL_1/ L_1 = DL_2/ L_2 \quad (6)$$

In the Sandercock interferometer, working at Perugia University, this condition is achieved mounting the interferometers on the same scanning stage, one with the mirror axis parallel to the scan direction, the other off set by an angle a. It is clear that the spacings of the two interferometers satisfy the equation $L_2=L_1 cos a$.

Figure 7 shows a schematic diagram of the whole experimental apparatus used for a BLS experiment in the backscattering configuration, which is usually exploited in the case of experiments on thin films and layered structures. In addition to the box containing the tandem-multipass interferometer and the optical components necessary for the multipass operation (3+3 passes in our case), one can see the external optics which is needed to focus the incident laser beam onto the surface of the specimen. In backscattering geometry the same lens (usually a commercial camera objective) is used to focus light and to collect the back-scattered photons for analysis through the interferometers. In this geometry, due to the conservation of the wavevector component parallel to the film surface, the wavevector of phonons revealed in the spectra is linked to the optical wavevector k_I by the simple relation:

$$q_{||} = 2\, k_I \sin q_i \qquad (7)$$

where q_i is the angle of incidence of light.

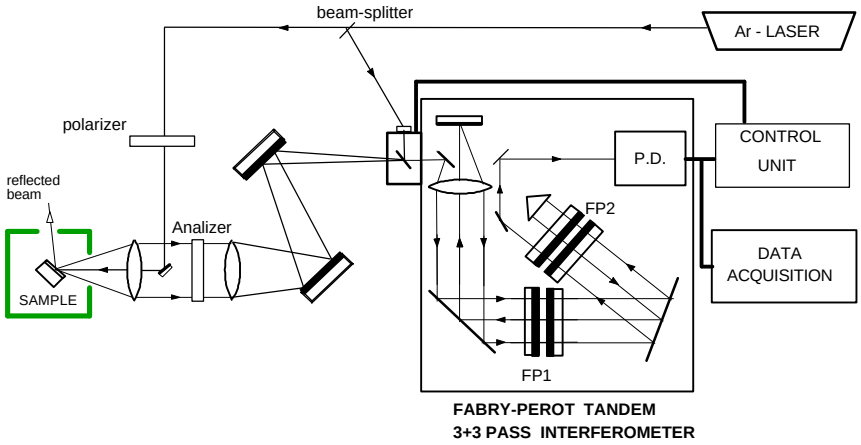

Fig. 7 Schematic view of the experimental apparatus used for BLS measurements.

4.2 Guided acoustic modes

Due to the above mentioned conservation of momentum in the phonon-photon interaction, the phonons involved in BLS experiments have wavelengths comparable with that of light, i.e. much larger than interatomic distances. Therefore the problem of acoustic propagation in a film/substrate structure can be solved within the theory of elasticity, by writing the equation of motion for the acoustic displacement field in terms of stress, strain and elastic stiffness constants. Now, as discussed above, in the case of BLS, the q// is fixed by the experimental geometry. Therefore one can write down the solution for the acoustic displacement field as a superposition of partial waves, characterised by the same value of q//. The amplitude of each partial wave is determined by imposing the boundary conditions and the free surface and at the interface. These boundary conditions are:

- the vanishing of the stress at the free surface;
- the continuity of the stress and of the strain at the interface.

In such a way, one can write down a homogeneous system of equations, whose determinant must vanish in order to find the solution. It can be shown that in the case of a isotropic film on a substrate (with the substrate material stiffer than the film material), a number of discrete acoustic modes exist, namely:

- the Rayleigh and Sezawa acoustic modes , which are polarized in the sagittal plane, between the phase velocity of shear vertical waves in the substrate and the surface wave velocity of the film material;
- the Love modes, polarized in the transverse direction (shear horizontal), which exist in the velocity interval between the shear horizontal phase velocity of the substrate and that of the film.

In a BLS experiment, the incoming monochromatic light can exchange energy and momentum with acoustic phonons, undergoing inelastic scattering. Both Stokes (phonon creation) and anti-Stokes (phonon annihilation) have the same probability, because at room temperature the phonon states occurring in this process are populated thanks to the thermal energy. The mechanisms of interaction of light and phonons are the following two:

- the rippling induced by the phonons at the free surface and at the interface;
- the elasto-optical interaction within the film and the substrate material.

The former effect is stronger in the case of a large refractive index variation at the surface or at the interface; the strength of the latter, on the other hand, depends on the value of the elasto-optical coefficients of the media involved. One important point to be considered is that, depending on both the geometrical and the optical parameter under consideration, these different mechanisms can interfere either constructively or destructively.

4.3 Measured spectra

Figs. 8 shows two typical BLS spectra measured from two of the specimens studied. It can be seen that a number of discrete peaks can be recognised, corresponding to the Rayleigh (R) and Sezawa (S) modes. Unfortunately, due to the above mentioned interference effects, some of the modes exhibit a very low cross section for a given film thickness and angle of incidence. We have taken measurements at different incidence angles for all the six specimens analysed (TEOS as prep. and annealed; HDP high D/S as dep. and annealed, HDP low D/S as dep. and annealed). In order to have a good signal-to-noise ratio, acquisition times as long as a couple of days were necessary for each measurement. It can be seen that up to five discrete modes can be measured for a given incidence angle. The value of the phase velocity decreases with

increasing the angle, due to the dispersive nature of the modes. In the following table, the value of the phase velocity of the different guided modes, for the specimens PG02 and PG03 are summarised..

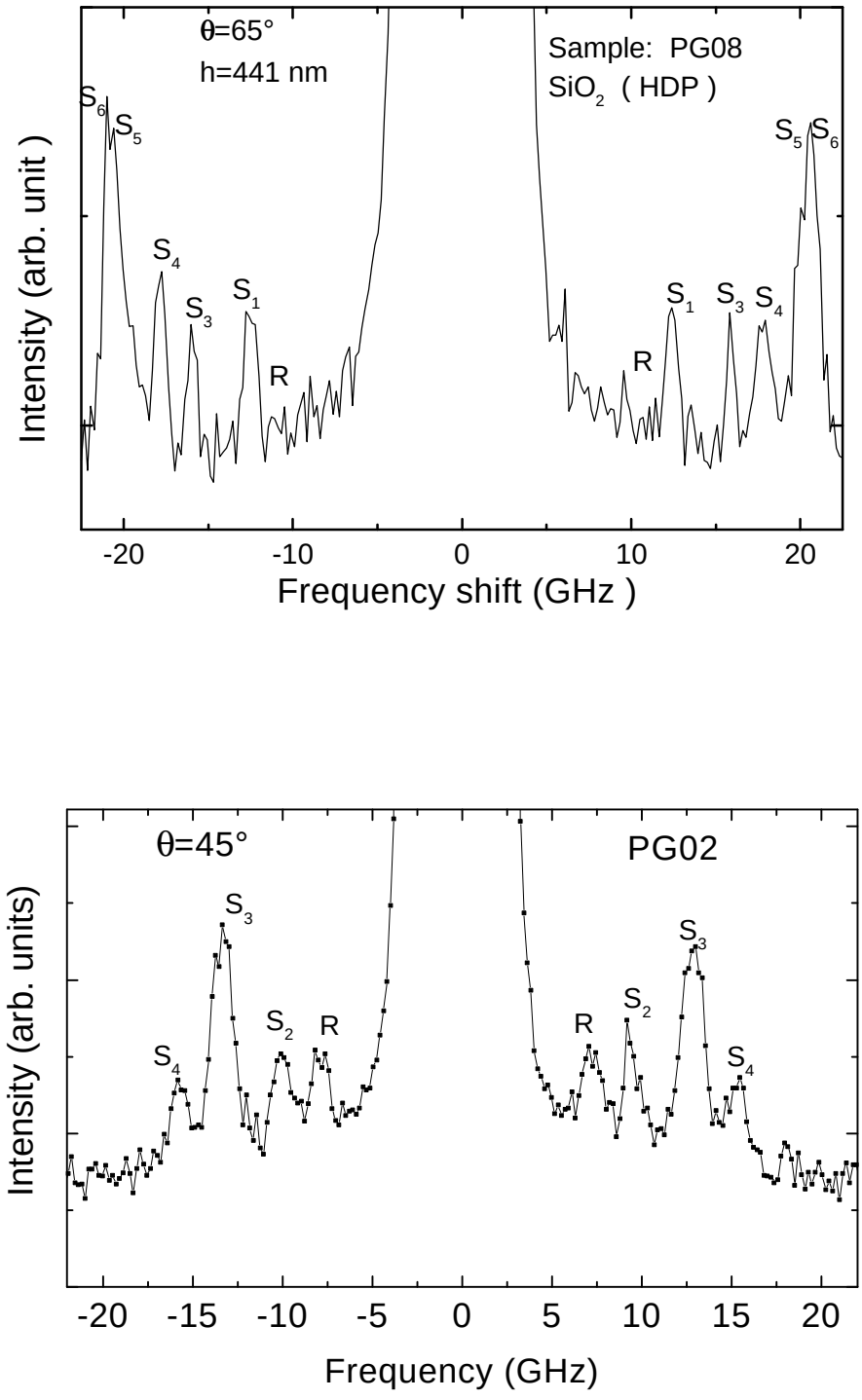

Fig. 8: BLS spectra from specimens PG02 and PG08.
The Rayleigh (R) and Sezawa (S) modes are indicated

Wafer	h (nm)	ρ (Kg/m)	θ (°)	Vr (m/s)	Vs1 (m/s)	Vs2 (m/s)	Vs3 (m/s)	Vs4 (m/s)	Vs5 (m/s)
TEOS As-prep.	485(5)	2370	45	2830(30)	3660(40)	4400(40)	4900(50)	5850(80)	
			55	2840(30)	3550(50)		4740(50)	5540(80)	
			65	2860(80)	3300(50)		4620(80)	5550(100)	
			70	2890(100)	3260(80)	4030(100)		5320(100)	5630(80)

Table 5: Experimental values of the phase velocities of guided modes for sample Perugia 2

Wafer	h (nm)	ρ (Kg/m)	θ (°)	Vr (m/s)	Vs1 (m/s)	Vs2 (m/s)	Vs3 (m/s)	Vs4 (m/s)	Vs5 (m/s)
TEOS annealed	445(5)	2700	45			4270(80)	5060(60)	5840(80)	6820(100)
			50		3800(40)	4270(80)	4960(50)	5830(100)	6500(100)
			55		3710(60)		4860(60)	5360(60)	6000(200)
			65		3720(30)		4670(50)	5230(50)	5970(80)

Table 6: Experimental values of the phase velocities of guided modes for sample Perugia 3

4.4 Evaluation of the film elastic constants

In order to obtain the film elastic constants from the measured values of the phase velocities, during the last months we have written a computer program which numerically solves the acoustic problem described in the previous section. The values of the elastic constants can be taken as fitting parameters and a best fit procedure of the experimental velocities to the calculated ones can be performed, assuming the characteristics of the Si substrate, the mass density and the thickness of the film, the wavelength of the laser light and the angle of incidence as known quantities. In order to go further to the evaluation of the elastic constant, we are presently implementing an automatic fitting procedure. Being this automatic routine under construction, we have done a preliminary evaluation of the elastic constants by a try-and-error manual procedure which yielded the values reported below for samples Perugia 2 and Perugia 3. A comparison between the experimental points and the calculated dispersion curves for specimen Perugia 2 can be seen in Fig. 8

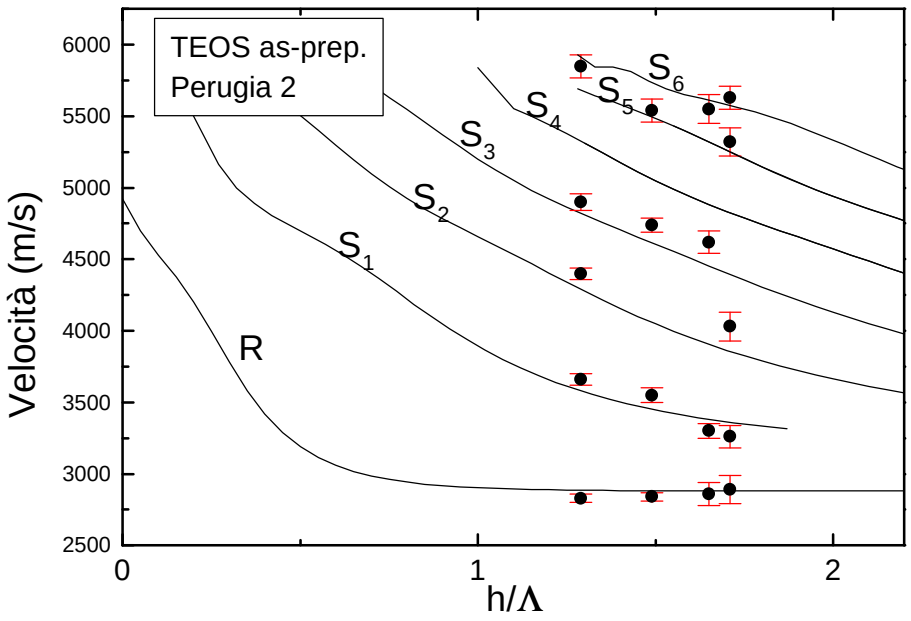

Fig. 8 Experimental (points) and calculated phase velocities of guided Rayleigh and Sezawa modes for sample Perugia 2, as a function of the ratio between film thickness and acoustic wavelength

From the values obtained for the elastic constants one can easily derive the Poisson's ratio ν and the Young's modulus E, which are related to c_{11} and c_{44} by the following classical expressions:

$$n = \frac{2c_{44} - c_{11}}{2(c_{44} - c_{11})} \qquad E = c_{11} - \frac{(c_{11} - 2c_{44})^2}{c_{11} - c_{44}}. \qquad (8)$$

From inspection of Table 7 it turns out that the elastic parameters of the Perugia 2 and Perugia 3 films are appreciably different due to the influence of the thermal treatment. In addition, they also differ significantly from those expected for fused silica. In particular, for the as prepared film, the Young's modulus is lower than in bulk silica and the Poisson's ratio is higher. For the annealed film E is similar to that of silica, but the Poisson's ratio is even bigger.

Once the automatic numerical fitting procedure will be completed, the elastic constants of all the films will be determined, aiming to study the role of different deposition conditions on the elastic properties of silicate glass films. The same numerical procedure will be applied, during the course of the STREAM project to determine the elastic constants of films of different materials, such as silicon nitride and different types of silicides which are in prduction.

Finally, we stress that measurements are going to be performed on silicate glass films as thick as 1 μm, in order to check the validity of isotropic elastic medium, assumed so far in the interpretation of the above measurements. In fact, for such quite thick films, it will be possible to detect bulk longitudinal waves propagating at different directions with respect to the surface normal and this will be very important in order to estimate the anisotropy of the films. We are also going to exploit X-ray reflectometry to have an independent estimate of the mass density of the films.

Sample	c_{11} *(GPa)*	c_{44} *(GPa)*	*E (GPa)*	*n*	*E/(1 - n) (GPa)*
Perugia 2	72±1.5	25.0±0.5	62±2	0.23±0.01	81±2
Perugia 3	86±1.5	28±1	70±2	0.26±0.01	95±3
Bulk silica	78.5	31.2	73	0.17	88

Table 7: Elastic moduli of the specimens Perugia 2 and Perugia 3, compared with those expected for bulk silica.

5. Conclusion

This characterization work allowed to define a measurement procedure to extract the film mechanical parameters necessary to simulate Shallow Trench Isolation process flow. In particular all mechanical parameters are available for TEOS oxide film. This work will be completed exploiting X-ray reflectometry to have an independent estimate of the mass density of the films and preparing thicker samples in order to check the validity of isotropic elastic medium. At the end the mechanical parameters for all the films will be available.

6. References

[1] S.M.SZE “VLSI Technology” pg 128 McGRAW-HILL INTERNATIONAL EDITIONS

[2] FLX 2400 OPERATION MANUAL, pg 33 TENCOR INSTRUMENTS

[3] ATHENA User’s Manual Appendix B pg 3 SILVACO International

7. Acknowledgments

The authors would like to thank Simona Spadoni, Enrico Bellandi for the contribution on dielectric thickness measurements and Daniele Caputo for the stress characterization on the samples.